

---

---

# Interface-Capturing Method for Calculating Transport Equations for a Multicomponent Heterogeneous System on Fixed Eulerian Grids

Ch. Zhang<sup>a, \*</sup> and I. S. Menshov<sup>a, b, \*\*</sup>

<sup>a</sup>*Moscow State University, Moscow, 119991 Russia*

<sup>b</sup>*Keldysh Institute of Applied Mathematics, Russian Academy of Sciences, Moscow, 125047 Russia*

\**e-mail: zhang-c@mail.ru*

\*\**e-mail: menshov@kiam.ru*

Received June 18, 2018; revised June 18, 2018; accepted November 19, 2018

**Abstract**—In this paper, we consider a new numerical method for solving the transport equations for a multicomponent heterogeneous system on fixed Eulerian grids. The system consists of an arbitrary number of components. Any two components are separated by a boundary (interface). Each component is determined by a characteristic function, i.e., a volume fraction that is transported in a specified velocity field and determines the spatial instantaneous component distribution. A feature of this system is that its solution requires two conditions to be met. Firstly, the volume fraction of each component should be in the range  $[0, 1]$ , and, secondly, any partial sum of volume fractions should not exceed unity. To ensure these conditions, we introduce special characteristic functions instead of volume fractions and propose solving transport equations with respect to them. It is proved that the fulfillment of these conditions is ensured when using this approach. In this case, the method is compatible with various TVD schemes (MINMOD, Van Leer, Van Albada, and Superbee) and interface-sharpening methods (Limited downwind, THINC, Anti-diffusion, and Artificial compression). The method is verified by calculating a number of test problems using all of these schemes. The numerical results show the accuracy and reliability of the proposed method.

*Keywords:* Eulerian grid, transport, multicomponent flow, interface-sharpening method

**DOI:** 10.1134/S2070048219060012

## INTRODUCTION

The multimaterial flow is encountered in various applications and applied problems. For example, an underwater explosion, the outflow of oil products or natural gas from an underwater pipeline, high-speed impact problems, and dynamic processes in heterogeneous multiphase media. In a multimaterial flow, there are different materials that are separated by interphase boundaries (interfaces), have various physical and mechanical properties, and are described by different equations of state. Direct modeling of such inhomogeneous flows involves calculating the flow parameters in internal homogeneous subdomains and the position of interphase boundaries at each time instant. Under strong spatial changes in the interphase boundaries, the subdomains of the homogeneous material and grids associated with them can also undergo strong deformations, in which the accuracy of the calculation deteriorates, resulting in unphysical results. For example, such a situation arises when simulating the Richtmyer-Meshkov instability that develops at the interphase boundary of two materials during the passage of a shock wave.

To circumvent the difficulties of direct numerical modeling associated with the deformation of the interphase boundary, there exists an alternative approach that is called the diffuse interface method in the literature. In this approach a medium of different materials is considered as a homogeneous, effective medium, the properties of which depend on the characteristic functions that determine the spatial component distribution. As a rule, the volume fraction of the component is used as such a function. The interphase boundary in this case is represented by a zone, where the value of the volume fraction varies from zero to unity.

Thus, the methods for calculating multimaterial flows can be divided into two groups: interface-tracking methods [1–5] and diffuse interface methods [6–9]. In the methods of the first group, the interphase

boundary is defined in a special way, and its position at each time step is calculated. In the methods of the second type, a interface-capturing calculation throughout the domain is carried out without the specification of a boundary. In this case, the interphase boundary is determined by the subdomain where the volume fraction is greater than zero and less than unity. The simulation accuracy in the second approach directly depends on the size of the interface zone. Therefore, an important problem is the development of computing technique that helps minimize the size of the smeared interface. At present, several such methods have been developed. They include the LD (Limited Downwind) method [10, 11], THINC method [12], AntiD (Anti-diffusion) method [13, 14], and ACM (Artificial Compression Method) method [15, 16]. These methods were initially developed for the case of two components. Their direct generalization to the case of  $N$  ( $N \geq 3$ ) components is impossible due to the appearance of an additional restriction on the values of volume fractions, i.e., compatibility conditions; in other words, the volume fraction of each component should be in the range  $[0, 1]$  and any partial sum of volume fractions should be less than unity. We will show that even the MUSCL scheme does not guarantee the fulfillment of this condition in the simple advection of three or more components.

The fulfillment of the compatibility condition depends on the numerical method used for solving the transport equations for the volume fractions of the components. Therefore, in this paper, we consider only the transport equations in a specified velocity field. The developed methods can be easily extended to the full system of Euler equations.

To ensure the compatibility condition for volume fractions in the case of  $N \geq 3$ , S. Jaouen [10] modified the numerical flux in the LD method [11]. In this case, a complex recursive procedure that works exclusively with the LD scheme was proposed.

In this paper, we propose a new approach that, unlike [10], is not associated with a specific numerical method for solving the transport equation. It is compatible with any of the interface-sharpening methods noted above. Instead of volume fractions in the transport equation, we propose using special characteristic functions, which are nonlinear combinations of volume fractions that automatically ensure the compatibility conditions, provided that the basic scheme for solving the equation is TVD.

## 1. PROBLEM STATEMENT

Let us consider the advection in the  $\mathbf{u}$  velocity field of a heterogeneous system of  $N$  components characterized by volume fractions of components  $z_i$ :

$$\partial_t z_i + \mathbf{u} \cdot \nabla z_i = 0, \quad i \in \Omega = \{1, 2, 3, \dots, N\}. \quad (1)$$

Due to normalization

$$\sum_{i=1}^N z_i = 1, \quad (2)$$

only  $(N - 1)$  unknowns are independent, and, accordingly, only  $(N - 1)$  transport equations need to be solved. The component not included in the system will be simply determined from (2). Without loss of generality, we will consider the following system:

$$\partial_t z_i + \mathbf{u} \cdot \nabla z_i = 0, \quad i \in \{2, 3, \dots, N\}. \quad (3)$$

The compatibility conditions for volume fractions are represented by the following inequalities:

$$z_i \in [0, 1], \quad (4)$$

and

$$\sum_j z_j \leq 1, \quad j \in \Lambda \subset \Omega. \quad (5)$$

If the initial data that satisfy inequalities (4) and (5) are specified at the initial moment of time, the solution on subsequent time layers must also satisfy these inequalities. The first-order standard upwind scheme ensures the fulfillment of the compatibility conditions. However, in this case, due to the large numerical viscosity, the discontinuities in the volume fractions suffer from strong numerical smearing, because of which it is difficult to clearly distinguish the interphase boundary. Higher order schemes, such as van Leer's MUSCL scheme with the MINMOD derivative limiter, based on the nonlinear interpolation significantly reduce the smear zone but do not ensure the fulfillment of the compatibility conditions.

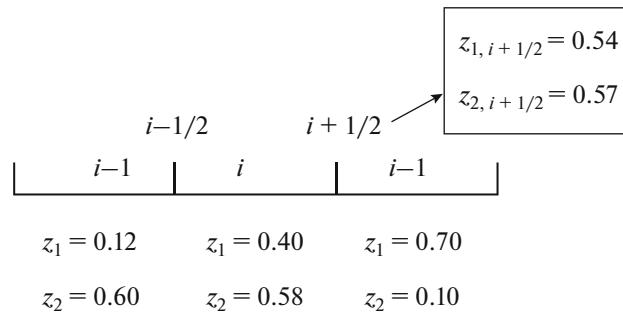


Fig. 1. MINMOD interpolation example for a system with three components.

This is because the interpolated values of volume fractions may violate conditions (4) and (5). Let us explain the root of the problem with the following example.

Figure 1 shows an example of MINMOD interpolation for a three-component system. Interpolation is performed for volume fractions at boundary  $i + 1/2$  between two cells indexed  $i$  and  $i + 1$ . Although the values of the volume fractions in the cells satisfy conditions (4) and (5), the interpolated values at boundary  $i + 1/2$  violate condition (5). The same problem arises when using other interface-sharpening methods.

In the first-order scheme, the compatibility conditions will not be violated since the volume fractions at the boundary are equal to the average volume fractions of either the left cell or the right cell. Therefore, the conditions are automatically satisfied at the boundary.

### 2. NEW CHARACTERISTIC FUNCTIONS

In order to fulfill the compatibility conditions when solving equation (1) with high-order schemes, we propose introducing special characteristic functions and solving transport equations with respect to them:

$$\partial_t f_i + \mathbf{u} \cdot \nabla f_i = 0, \quad i \in \{2, 3, \dots, N\}, \tag{6}$$

where

$$f_i = f_i(z_{i-1}, z_i, \dots, z_N) = \frac{\sum_{k=i}^N z_k}{\sum_{k=i-1}^N z_k}. \tag{7}$$

In the particular case of  $N = 3$ , the characteristic functions have the following form:

$$f_2 = \frac{z_2 + z_3}{z_1 + z_2 + z_3} = z_2 + z_3, \quad f_3 = \frac{z_3}{z_2 + z_3}.$$

*Lemma 1. The system of equations (3) and the system of equations (6) are equivalent if*

$$z_i \neq 0, \quad i \in \{2, 3, \dots, N\}.$$

*Proof.* We rewrite Eq. (6) as follows:

$$\partial_t f_i(z_2, z_3, \dots, z_N) + \mathbf{u} \cdot \nabla f_i(z_2, z_3, \dots, z_N) = \sum_{i=2}^N \frac{\partial f_i(z_2, z_3, \dots, z_N)}{\partial z_k} (\partial_t z_k + \mathbf{u} \cdot \nabla z_k) = 0. \tag{8}$$

After simple calculations, we find the Jacobian

$$J = \begin{vmatrix} \partial f_2 / \partial z_2 & \partial f_2 / \partial z_3 & \dots & \partial f_2 / \partial z_N \\ \partial f_3 / \partial z_2 & \partial f_3 / \partial z_3 & \dots & \partial f_3 / \partial z_N \\ \vdots & \vdots & \vdots & \vdots \\ \partial f_N / \partial z_2 & \partial f_N / \partial z_3 & \dots & \partial f_N / \partial z_N \end{vmatrix} = \frac{1}{\prod_{i=2}^{N-1} \left( \sum_{k=i}^N z_k \right)}. \tag{9}$$

Since  $z_i \neq 0, i \in \{2, 3, \dots, N\}$ , the Jacobian is not equal to zero. This means that the system of equations (3) and the system of equations (6) are equivalent. ■

If a certain component is absent in the computational cell and its volume fraction is zero, the Jacobian and characteristic functions acquire a singularity. To avoid such degeneracy, a small value of  $\eta$  (for exam-

ple,  $\eta = 10^{-6}$ ), which limits the components from total degeneracy, is introduced. Thus, in the model under consideration, the absence of a component actually means its presence, albeit, in a negligible amount. Complete degeneration of the component is not allowed.

Since the system of equations (3) and the system of equations (6) are equivalent, their exact solutions coincide. Therefore, at the convergence of the numerical scheme, the numerical solutions will be close to each other and coincide in the limit.

*Lemma 2.* *Let there be values of volume fractions satisfying the compatibility conditions (4) and (5) and an interpolation scheme that preserves monotonicity during the subcell reconstruction. Then the application of such a scheme to the values of the characteristic functions (7) determines the interpolated values of the volume fractions that also satisfy the compatibility conditions (4) and (5).*

*Proof.* Since the averaged values of the volume fractions satisfy conditions (4) and (5), we have for the averaged values of the characteristic functions

$$f_{i,j} \in [0,1], \tag{10}$$

where  $i$  is the index of the component and  $j$  is the index of the cell.

If an interpolation scheme that preserves monotonicity is used, then a new extreme is not produced, i.e.,

$$f_i^{cf} \in [0,1], \tag{11}$$

where the superscript cf denotes the interpolated values. The interpolated values of the characteristic functions and volume fractions are related by the following relation:

$$f_i^{cf} = \sum_{k=i}^N z_k^{cf} / \sum_{k=i-1}^N z_k^{cf} \in [0,1], \quad i \in \{2,3,\dots,N\}, \tag{12}$$

from which we obtain at once that

$$0 \leq z_N^{cf} \leq \sum_{k=N-1}^N z_k^{cf} \leq \dots \leq \sum_{k=3}^N z_k^{cf} \leq \sum_{k=2}^N z_k^{cf} \leq 1. \tag{13}$$

Inequality (13) ensures the fulfillment of conditions (4) and (5). ■

Thus, having solved the system of equations (6), numerical solutions of the system (3) that satisfy the requirements (4) and (5) can be found. For this purpose, the volume fractions must be expressed in terms of the characteristic functions. Solution (7) gives simple formulas for this transformation:

$$z_i = \prod_{k=2}^i f_k - \prod_{k=2}^{i+1} f_k, \quad i < N, \quad z_N = \prod_{k=2}^N f_k. \tag{14}$$

If the TVD scheme is used to solve the transport equation in the characteristic functions, then their full variations will decrease in time, i.e.,

$$[\text{TV}(f_i)]^{n+1} \leq [\text{TV}(f_i)]^n, \tag{15}$$

where the full variation is determined by the following formula:

$$\text{TV}(f_i) = \sum_j |f_{i,j+1} - f_{i,j}|. \tag{16}$$

However, it is not obvious that the TVD of the characteristic functions also ensures the TVD property of the volume fractions. The monotonicity of the characteristic functions do not necessarily ensure the monotonicity of the volume fractions. Nevertheless, it can be proved that the total variation in the volume fraction remains limited. For this purpose, we first need to prove the following lemma.

*Lemma 3.* *The complete variation of the product of two characteristic functions is limited by the following inequality:*

$$\text{TV}(f_m f_l) \leq \text{TV}(f_m) + \text{TV}(f_l). \tag{17}$$

**Proof.**

$$\begin{aligned} \text{TV}(f_l f_m) &= \sum_j |(f_l f_m)_{j+1} - (f_l f_m)_j| = \sum_j |(f_l)_{j+1} [(f_m)_{j+1} - (f_m)_j] + (f_m)_j [(f_l)_{j+1} - (f_l)_j]| \\ &\leq \sum_j |(f_l)_{j+1} [(f_m)_{j+1} - (f_m)_j]| + \sum_j |(f_m)_j [(f_l)_{j+1} - (f_l)_j]|. \end{aligned} \tag{18}$$

Since  $0 \leq (f_l)_{j+1}, (f_m)_j \leq 1$ , we obtain that

$$\begin{aligned} \text{TV}(f_l, f_m) &\leq \sum_j |(f_l)_{j+1}| [(f_m)_{j+1} - (f_m)_j] + \sum_j |(f_m)_j| [(f_l)_{j+1} - (f_l)_j] \\ &\leq \sum_j |(f_m)_{j+1} - (f_m)_j| + \sum_j |(f_l)_{j+1} - (f_l)_j| = \text{TV}(f_l) + \text{TV}(f_m). \quad \blacksquare \end{aligned} \tag{19}$$

*Lemma 4.* The complete variation of the volume fraction  $z_i$  is limited by the following inequalities:

$$\text{TV}(z_i) \leq C_i, \quad C_i^{n+1} \leq C_i^n. \tag{20}$$

*Proof.* Using Eq. (14) and Lemma 3, we obtain

$$\text{TV}(z_i) = \sum_{k=2}^i \text{TV}(f_k) + \sum_{k=2}^{i+1} \text{TV}(f_k) = C_i, \quad i < N \tag{21}$$

and

$$\text{TV}(z_N) = \text{TV}\left(\prod_{k=2}^N f_k\right) = \sum_{k=2}^N \text{TV}(f_k) = C_N. \tag{22}$$

From inequality (15), it follows that  $C_i^{n+1} \leq C_i^n, i \in \{2, 3, \dots, N\}$ .  $\blacksquare$

Lemma 4 means that, although the complete variation in the volume fraction does not decrease, it is nevertheless limited by an upper limit decreasing in time.

**Comment.** The characteristic functions (7) are not the only choice. The following combinations also ensure the fulfillment of the compatibility conditions (4) and (5):

$$f_i = f_i(z_{i-1}, z_i, \dots, z_N) = \frac{\sum_{k=i}^N \Psi(z_k)}{\sum_{k=i-1}^N \Psi(z_k)}, \tag{23}$$

$$f_i = f_i(z_{i-1}, z_i, \dots, z_N) = \Psi\left(\frac{\sum_{k=i}^N z_k}{\sum_{k=i-1}^N z_k}\right), \tag{24}$$

where  $\Psi(x) \in [0, 1], x \in [0, 1]$ , is a monotonic function. For example,  $\Psi(x) = x^\beta, \beta \in \mathbb{R}^+$ .

### 3. DISCRETIZATION

The explicit scheme and the finite volume method are used to discretize the system of Eqs. (3) and (6):

$$q^{n+1} = q^n - u\lambda(q_{j+1/2}^n - q_{j-1/2}^n), \tag{25}$$

where  $\lambda = \Delta t / \Delta x$ ,  $\Delta t$ , and  $\Delta x$  are time steps and space steps, respectively,  $u$  is the speed, and superscripts  $n$  and  $n + 1$  denote the corresponding time step. Below, superscript  $n$  is omitted for simplicity.

We analyze two approaches when  $q = z_i$  and  $q = f_i$  are taken as unknown quantities. In both cases, the characteristic functions (7) are used for subcell interpolation in order to satisfy the compatibility conditions (4) and (5). An upwind scheme is used to calculate the numerical flow, i.e.,

$$q_{j+1/2} = \frac{u + |u|}{2} q_{j+1/2,L} + \frac{u - |u|}{2} q_{j+1/2,R}, \tag{26}$$

where  $q_{j+1/2,L}$  and  $q_{j+1/2,R}$  are the interpolated  $q$  values on the left and right sides of the boundary between cells  $j$  and  $j + 1$ .

In the next section, we compare the proposed method with the method of S. Jaouen [10] developed based on the LD scheme [11]. The latter is actually equivalent to the Ultrabee scheme for the linear transport equation. In order to satisfy the compatibility conditions, a rather cumbersome modification of the

numerical flow LD is proposed in [10]. The transport equations for  $q = z_i$  are considered, and the numerical flow is determined as follows:

$$z_{i,j+1/2} = \begin{cases} d_{i,j+1/2}, & z_{i,j+1/2} < d_{i,j+1/2} \\ z_{i,j+1}, & d_{i,j+1/2} \leq z_{i,j+1/2} \leq D_{i,j+1/2} \\ D_{i,j+1/2}, & z_{i,j+1/2} > D_{i,j+1/2}. \end{cases} \quad (27)$$

$$m_{i,j+1/2} = \min(z_{i,j}, z_{i,j+1}), \quad M_{i,j+1/2} = \max(z_{i,j}, z_{i,j+1}),$$

$$\begin{aligned} b_{i,j+1/2} &= \frac{z_{i,j} - M_{i,j-1/2}}{u\lambda} + M_{i,j-1/2}, \quad B_{i,j+1/2} = \frac{z_{i,j} - m_{i,j-1/2}}{u\lambda} + m_{i,j-1/2}, \\ a_{i,j+1/2} &= \max(b_{i,j+1/2}, m_{i,j+1/2}), \quad A_{i,j+1/2} = \min(B_{i,j+1/2}, M_{i,j+1/2}), \\ d_{i,j+1/2} &= \max\left(a_{i,j+1/2}, 1 - \sum_{l=2}^N A_{l,j+1/2}\right), \quad D_{i,j+1/2} = \min\left(A_{i,j+1/2}, 1 - \sum_{l=2}^N a_{l,j+1/2}\right), \\ d_{i,j+1/2} &= \max\left(a_{i,j+1/2}, 1 - \sum_{l=1}^{i-1} z_{l,j+1/2} - \sum_{l=i+1}^N A_{l,j+1/2}\right), \quad i \in \{2, 3, \dots, N-1\}, \\ D_{i,j+1/2} &= \min\left(A_{i,j+1/2}, 1 - \sum_{l=1}^{i-1} z_{l,j+1/2} - \sum_{l=i+1}^N a_{l,j+1/2}\right), \quad i \in \{2, 3, \dots, N-1\}. \end{aligned} \quad (28)$$

Obviously, the method [10] is much more complicated than the characteristic functions-based approach proposed in the present work. Furthermore, it is strongly associated with the LD scheme. Our method does not imply any special interface-sharpening scheme. It is compatible with any of the above nonlinear interpolation methods without any modifications.

#### 4. NUMERICAL TESTS

In this section, the proposed method of characteristic functions is tested on some one-dimensional and two-dimensional transport problems. Classical second-order TVD schemes, such as MUSCL with derivative limiters MINMOD, Van Albada, and Superbee, as well as special interface-sharpening algorithms, including LD, AntiD, THINC, and ACM, are considered and compared. By default, the Courant number was 0.2 in all the calculations.

##### 4.1. Three-Component System Advection

The calculated domain is the interval  $[0,1]$ . The initial component distributions are as follows:

$$z_1(x) = \frac{X_{[0.4,0.6]}(x)}{2}, \quad z_2(x) = |x - 1/2|, \quad z_3(x) = 1 - z_1(x) - z_2(x), \quad (29)$$

where the function  $X_I(x) = \begin{cases} 1, & x \in I, \\ 0, & x \notin I. \end{cases}$

Periodic boundary conditions apply on the left and right boundaries. The advection rate is  $u = 1$ . In this example, we do not consider the AntiD, THINC, and ACM schemes that are designed specifically for interface sharpening, where a sharp transition  $z_+ \rightarrow 0$ ,  $z_- \rightarrow 1$  or  $z_+ \rightarrow 1$ ,  $z_- \rightarrow 0$  occurs.

Figure 2 shows the initial distribution of the volume fractions of each component and the solution of the system of equations (3) obtained with the first-order upwind scheme. As can be seen in the figure, there is a strong distortion of the initial distributions due to the excessive numerical viscosity.

Second-order schemes reduce numerical viscosity. However, if they are applied to the transport equation for volume fractions, the nonlinear interpolation operator can lead to negative values, as can be seen in Fig. 3, which shows the numerical results of the solution using the MUSCL-Superbee and LD schemes.

Let us now consider the numerical solutions that are obtained if the proposed characteristic functions are used in the transport equation. The numerical solutions of the system of equations (6) obtained using

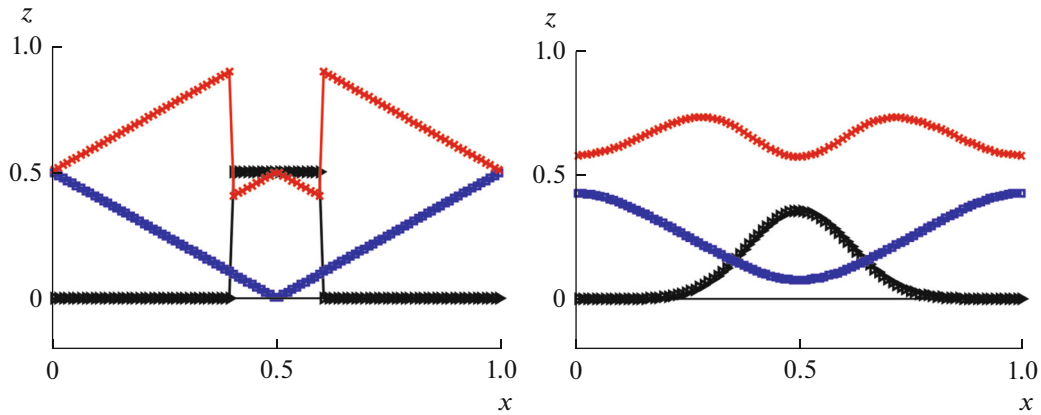


**Fig. 2.** Initial distribution of volume fractions (left) and numerical results obtained with the first-order upwind scheme after a single cycle,  $t = 1.0$  (right).  $\rightarrow z_1$   $\blacksquare z_2$   $\times z_3$ .

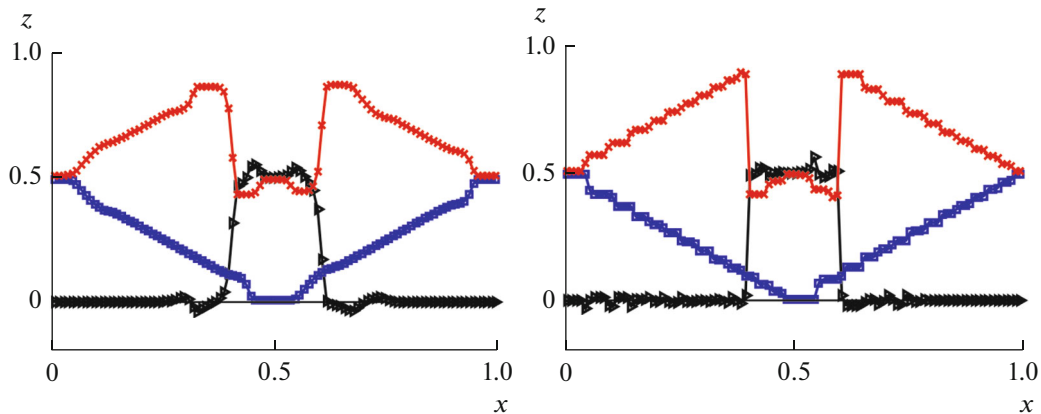


**Fig. 3.** Numerical results for Superbee (left) and LD (right) scheme after a single cycle,  $t = 1.0$ . The solution of equations (3) with respect to volume fractions.  $\rightarrow z_1$   $\blacksquare z_2$   $\times z_3$ .

the second-order MUSCL scheme with various derivative limiters (Minmod, Van Leer, Van Albada, and Superbee) and the LD scheme are shown in Figs. 4, 5, and 6, respectively. The results show that the resulting values of the volume fractions satisfy the compatibility conditions in all the tests. Negative volume fractions do not appear.

Figure 7 shows the results of the calculation of 500 cycles ( $t = 500$ ) with the characteristic functions and the LD scheme. For comparison, similar results by the method of S. Jaouen [10] are also presented. The results almost coincide. The total variations are shown in Fig. 8. As can be seen in the Fig. 8, the total variation barely changes with time in our method and the method [10].

#### 4.2. Interphase Boundary Transfer

This problem models the motion of interphase boundaries. Its formulation is schematically shown in Fig. 9. The computational domain is a segment  $[0.0\text{m}, 1.0\text{m}]$ . Inside the domain, the intervals  $I_1 = [0.0\text{m}, 0.2\text{m}]$ ,  $I_2 = [0.2\text{m}, 0.4\text{m}]$ ,  $I_3 = [0.4\text{m}, 0.6\text{m}]$ , and  $I_4 = [0.6\text{m}, 1.0\text{m}]$ , which contain the 1st, 2nd, 3rd, and 1st components of a three-component system at the initial time, are specified. The number of cells is 100. Periodic boundary conditions are specified on the left and right boundaries.

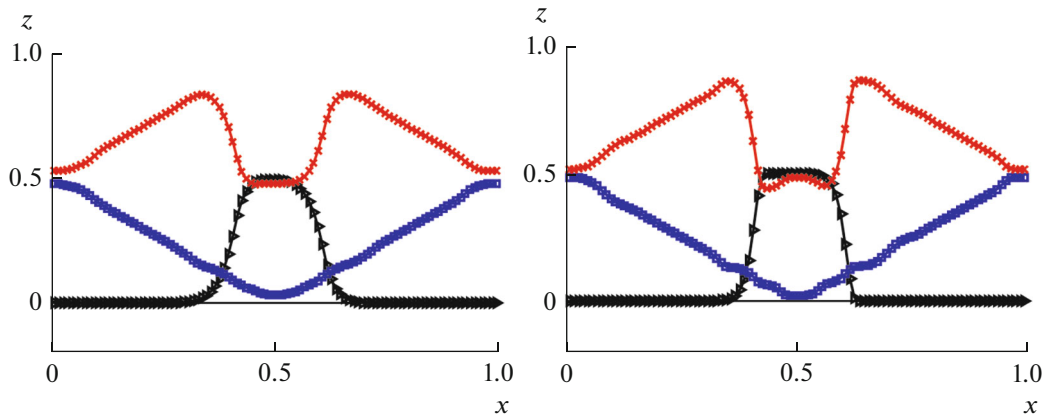


**Fig. 4.** Numerical results obtained with the MINMOD (left) and van Leer (right) schemes after a single cycle,  $t = 1.0$ . The solution of Eqs. (6) with respect to characteristic functions.  $\blacktriangleright z_1$   $\blacksquare z_2$   $\color{red}\times z_3$ .

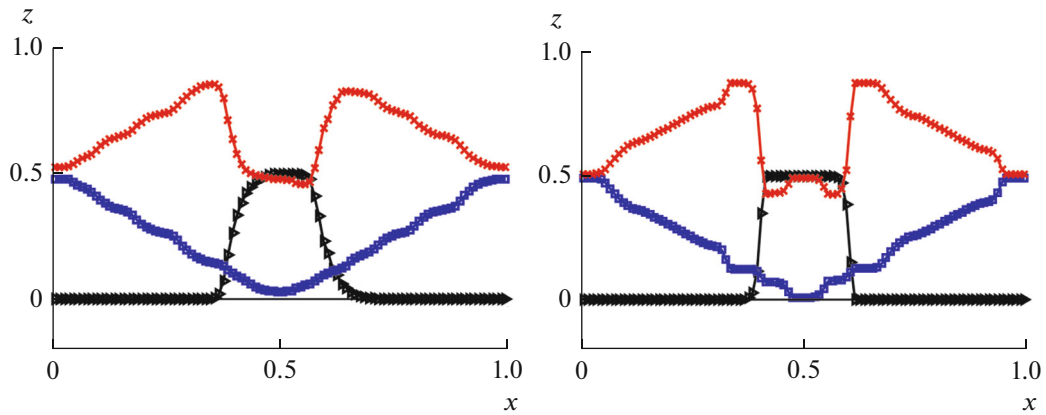


**Fig. 5.** Numerical results obtained with the van Albada (left) and Superbee (right) scheme after a single cycle,  $t = 1.0$ . The solution of Eqs. (6) with respect to characteristic functions.  $\blacktriangleright z_1$   $\blacksquare z_2$   $\color{red}\times z_3$ .

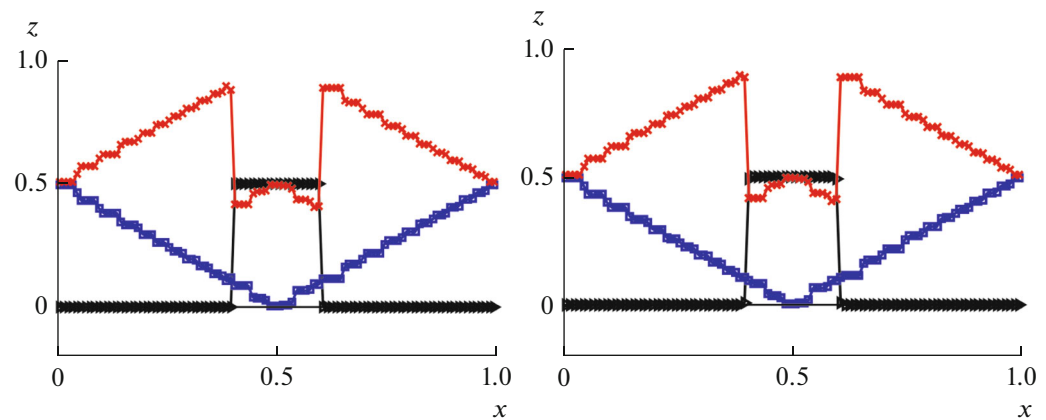


**Fig. 6.** Numerical results obtained with the LD scheme with characteristic functions (6) (left) and the S. Jaouen method [10] (right) after a single cycle,  $t = 1.0$ .  $\blacktriangleright z_1$   $\blacksquare z_2$   $\color{red}\times z_3$ .

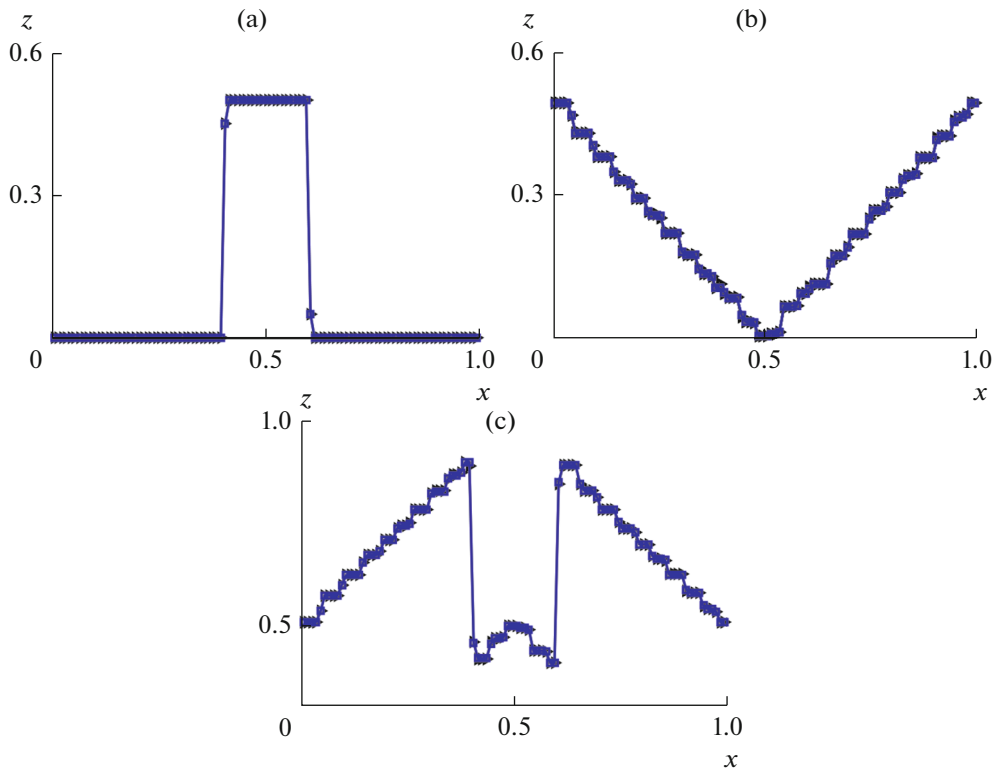


Fig. 7. Comparison of the LD method with characteristic functions and the S. Jaouen method [10]. Calculation of 500 cycles,  $t = 500$ : (a)  $z_1$ , (b)  $z_2$ , and (c)  $z_3$ .  $\blacktriangleright$  Our method  $\blacksquare$  Jaouen method

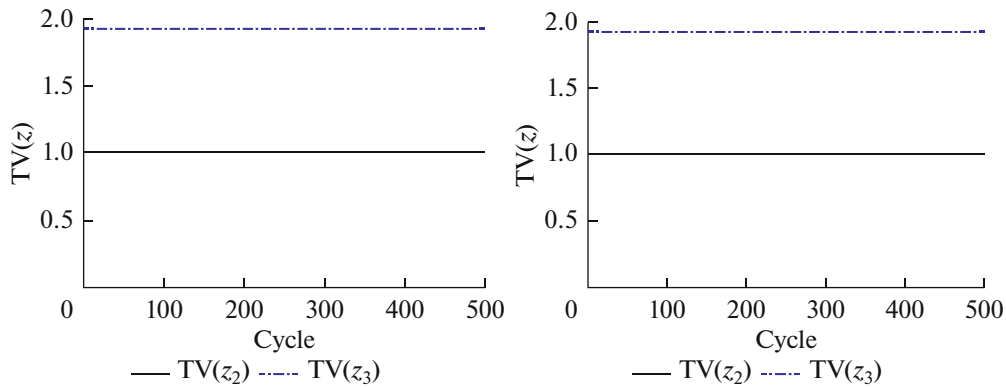


Fig. 8. Total variations of numerical solutions in the LD method with characteristic functions (left) and S. Jaouen method [10] (right). Calculation of 500 cycles ( $t = 500$ ).

The initial data is specified as follows:

$$z_1(x) = \Xi_{I \cup I_4}(x), \quad z_2(x) = \Xi_{I_2}(x), \quad z_3(x) = \Xi_{I_3}(x).$$

where  $\Xi_I(x) = \begin{cases} 1 - 10^{-6}, & x \in I \\ (1/(N - 1)) \times 10^{-6}, & x \notin I. \end{cases}$

In this problem, we test our method with the MINMOD, LD, THINC, AntiD, and ACM schemes. The numerical results after ten cycles are presented in Fig. 10. It can be seen that, except MINMOD, the interphase boundaries have a high resolution in 2–3 cells. In this case, the numerical oscillations associated with the violation of the compatibility conditions are not observed.

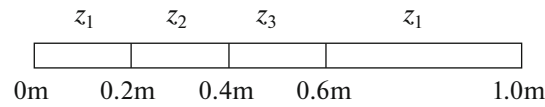


Fig. 9. Calculation scheme of the transport problem of the interphase boundary.

### 4.3. Transfer of Seven Components

Next, we consider a more computationally difficult problem, i.e., transport of a 7-component system. At the initial moment, each component is determined by the distribution of volume fractions that satisfy the compatibility conditions (4) and (5):

$$\begin{aligned}
 z_1(x) &= X_{[0,1/2]}(x)((1 + \sin(2\pi x))/10), & z_2(x) &= |x - 1/2|, \\
 z_3(x) &= (1.5 + \sin(0.7 + 2\pi x))/14, & z_4(x) &= 0.5 \exp(-100(x - 1/2)^2), \\
 z_5(x) &= (1 + \cos(10\pi x))/14, & z_6(x) &= (X_{[0.7,1]}(x))/7, & z_7(x) &= 1 - \sum_{k=1}^6 z_k(x).
 \end{aligned}
 \tag{30}$$

The initial distribution is shown in Fig. 11. The calculation is carried out on two grids with 100 and 1000 cells, respectively. The numerical results for the MINMOD and LD schemes are presented in Figs. 12 and 13. As expected, the more dissipative MINMOD scheme produces the greater distortion in the volume fraction distributions compared to the LD scheme, which shows excellent convergence. As can be seen in Fig. 13, the resolution of discontinuities in the LD scheme for 1000 cells is only one point. At the same time, our method of characteristic functions guarantees the compatibility conditions (4) and (5) in the numerical solutions both in MINMOD and in the LD scheme at various grid resolutions.

### 4.4. Two-Dimensional Transfer of a 4-Component System

The transport problem of a 4-component system, which is shown in Fig. 14, is considered. The system at the initial moment is represented by two circles ( $O_1, O_2$ ) and one cruciform region ( $C$ ), which are determined by the following formulas:

$$\begin{cases}
 O_1 = B((1,1), 0.5) \\
 O_2 = B((1,1), 0.7) \\
 C = [0.8, 1.2] \times [0.4, 1.6] \cup [0.4, 1.6] \times [0.8, 1.2].
 \end{cases}$$

The initial distribution of the volume fractions of the components has the following form:

$$\begin{aligned}
 z_1(x, y) &= \Xi_C(x, y), & z_2(x, y) &= \Xi_{O_1/C}(x, y), \\
 z_3(x, y) &= \Xi_{O_2/(C \cup O_1)}(x, y), & z_4(x, y) &= 1 - \sum_{k=1}^3 z_k(x, y).
 \end{aligned}$$

The following statements are considered: (a) the translation of materials along the diagonal with a speed  $u = (1,1)$  and (b) rotation around the point  $(1,1)$ . Five methods are tested: (1) LD, (2) THINC, (3) AntiD, (4) ACM, and (5) MUSCL.

Periodic boundary conditions are set at the boundaries. The calculation is carried out on a  $400 \times 400$  grid. The Strang dimensional splitting method is used. The numerical results after two cycles ( $t = 10$  s) of diagonal transfer are shown in Fig. 15a. In the results obtained by the MUSCL scheme, strong smearing of the interphase boundaries is observed. Other methods for interface sharpening effectively reduce the smear zone. The best interface resolution is provided by the LD method and the ACM.

In the AntiD scheme, the resolution of the interfaces is slightly worse than that in the other methods. In this case, the distribution of the volume fractions is distorted as a result of the transfer. It is possible to reduce the zone of the interphase boundary by repeatedly applying the AntiD scheme. However, this leads to an even stronger distortion of its shape.

The numerical solutions of the problem in the case of rotation obtained after two cycles ( $t = 2$  s) according to various schemes are presented in Fig. 15b. As can be seen from the presented results, the interfaces are most precisely resolved here also by the LD scheme. In the volume fraction distributions obtained by the THINC scheme, oscillations and a rather strong smearing of the interface are observed.

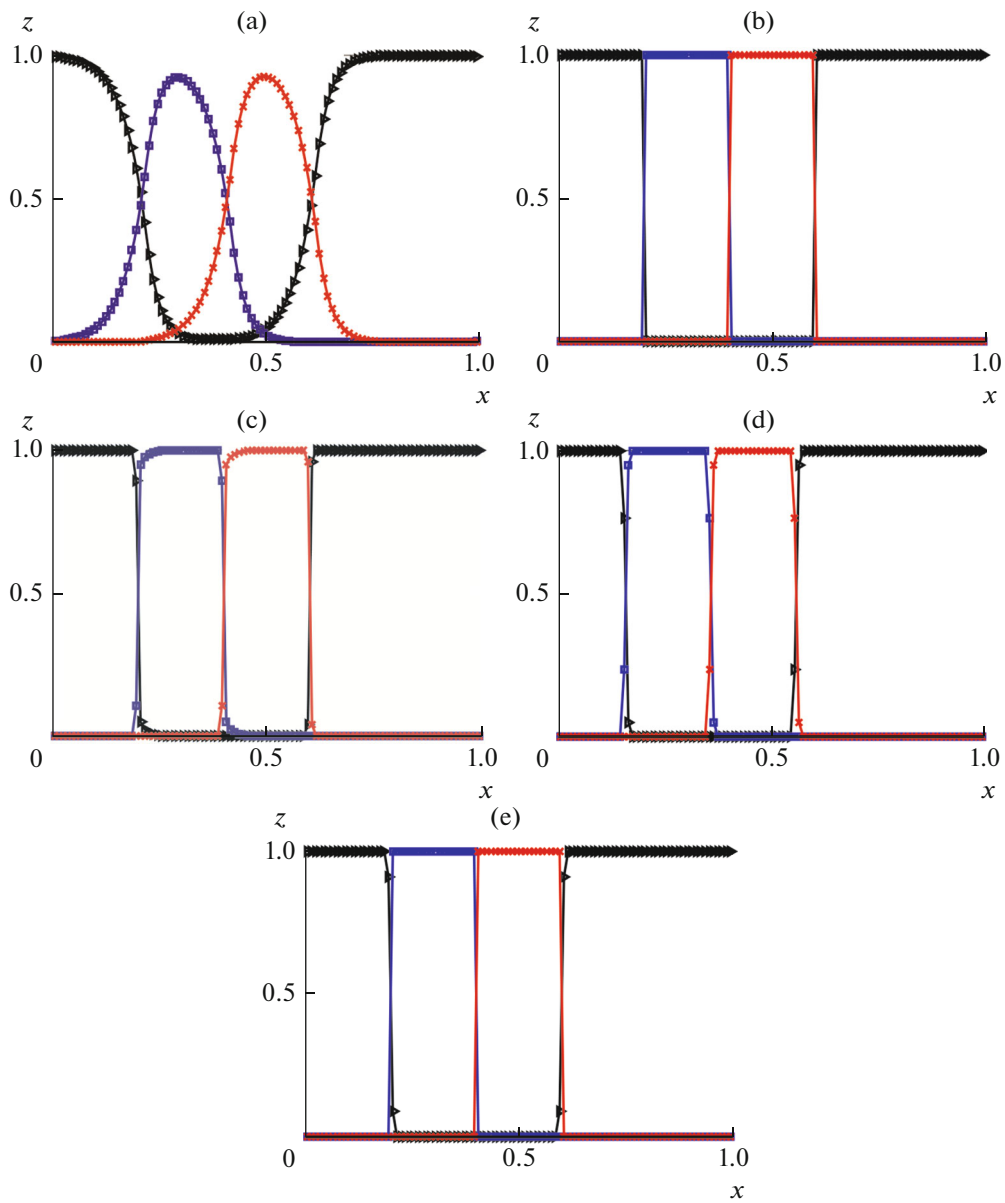


**Fig. 10.** Numerical results of the interface transport problem: (a) MINMOD scheme, (b) LD scheme, (c) THINC scheme, (d) AntiD scheme, and (e) ACM scheme.  $\blacktriangleright z_1$   $\blacksquare z_2$   $\blacktriangleright z_3$ .

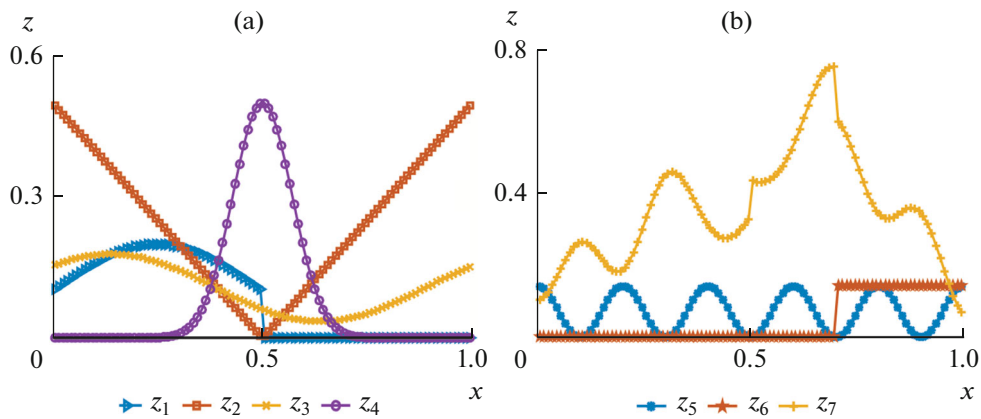


**Fig. 11.** Initial distribution of volume fractions in the transport problem of a 7-component system.

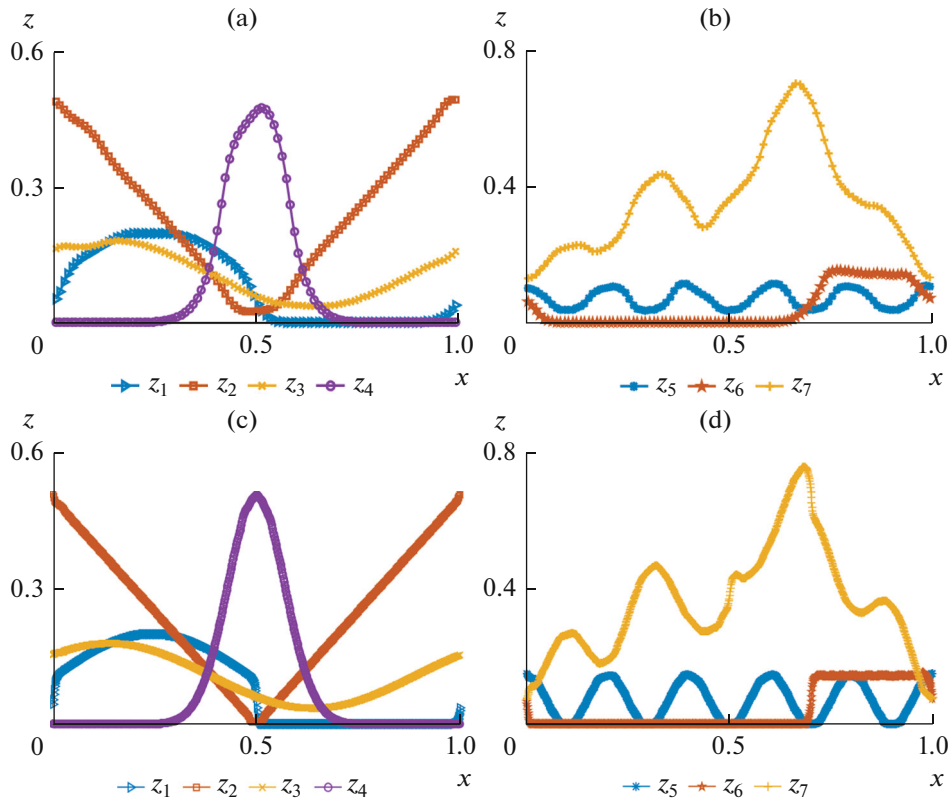


**Fig. 12.** Numerical results of the 7-component system transport problem obtained with the MINMOD scheme: (a, b) number of cells is 100, (c, d) number of cells is 1000.

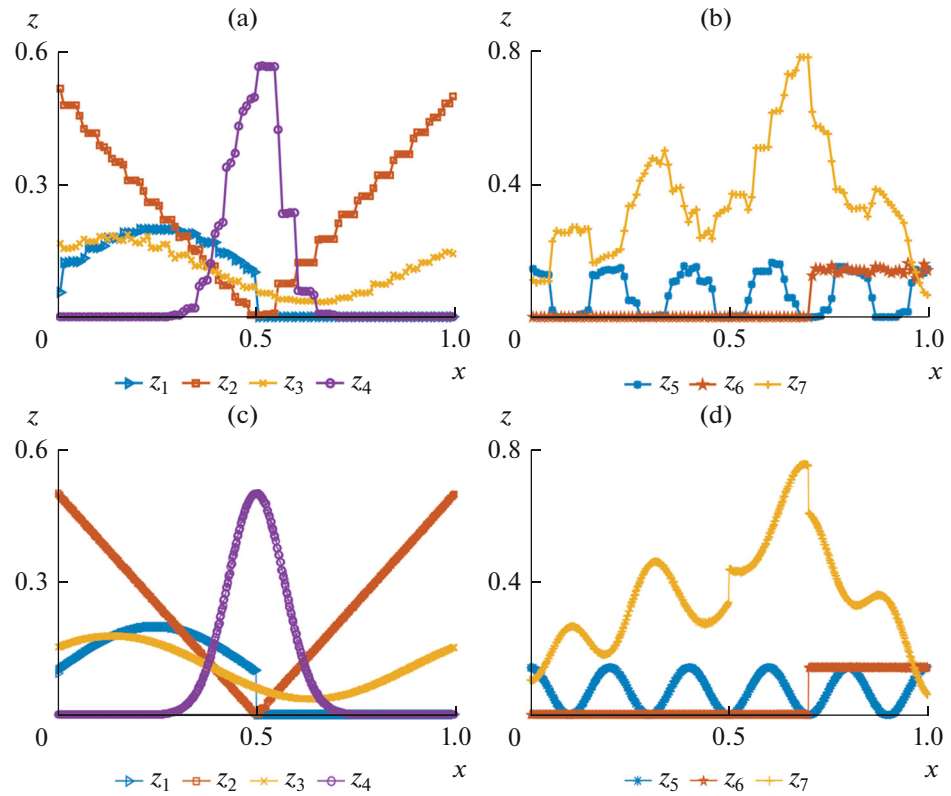


**Fig. 13.** Numerical results of the 7-component system transport problem obtained with the LD scheme: (a, b) number of cells is 100, (c, d) number of cells is 1000.

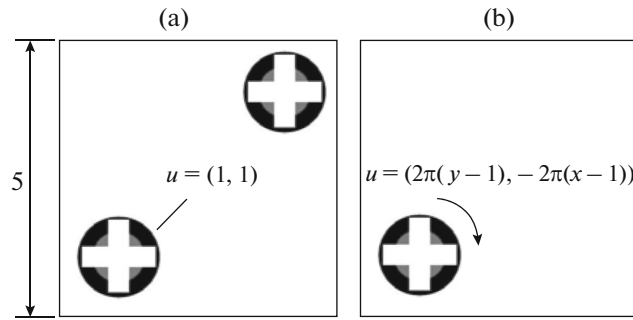


Fig. 14. Scheme of the two-dimensional transport problem of a 4-component system: (a) translation and (b) rotation.

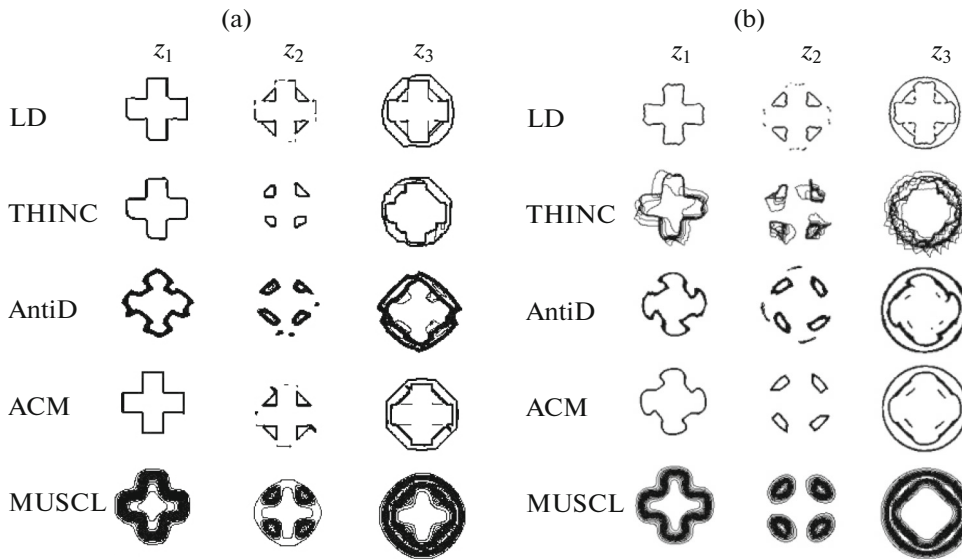


Fig. 15. Contour levels of volume fractions: (a) after two cycles of translation along the diagonal, (b) after two cycles of rotation.

In the volume fraction distributions obtained by the AntiD and ACM schemes, there are strong distortions of the material interfaces.

4.5. 4-Component System Transfer in a Vortex Field

In the last test, we consider the transfer of a 4-component system by a vortex velocity field. The initial distribution of the components is shown in Fig. 16. The length of the square side is 1.0. The center of the circle ( $\Omega_1 + \Omega_2$ ) is (0.50, 0.50) and the radius is 0.15. At the initial moment, there are four different components in the computational domain. Volume fractions are determined by the following formulas:

$$z_1(x, y) = \Xi_{\Omega_1}(x, y), \quad z_2(x, y) = \Xi_{\Omega_2}(x, y),$$

$$z_3(x, y) = \Xi_{\Omega_3}(x, y), \quad z_4(x, y) = 1 - \sum_{k=1}^3 z_k(x, y).$$

The velocity field is first determined by the vortex distribution with a clockwise direction,

$$u = \sin^2(\pi x) \sin(2\pi y), \quad v = -\sin^2(\pi y) \sin(2\pi x).$$

At the time moment  $t = 1.0$ , the direction of the velocity vector instantly changes to the opposite one, i.e., at  $t > 1.0$ , the distribution of the velocity vector becomes

$$u = -\sin^2(\pi x) \sin(2\pi y), \quad v = \sin^2(\pi y) \sin(2\pi x).$$

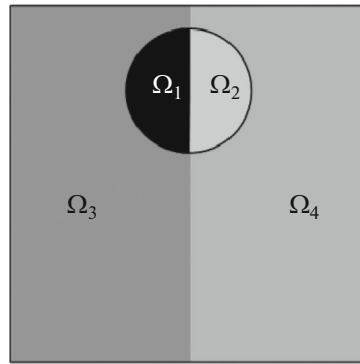


Fig. 16. Scheme of the transport problem in a vortex velocity field.

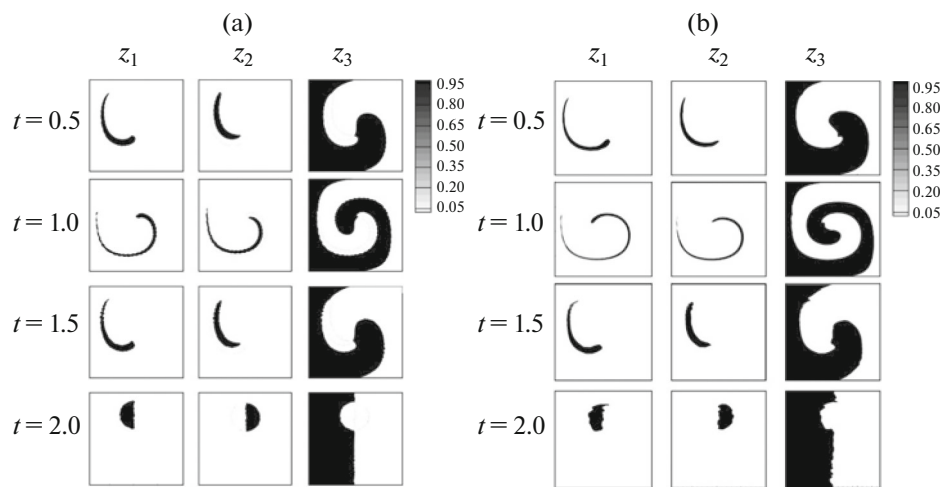


Fig. 17. Distributions of volume fractions obtained at various times:  $t = 0.5, 1.0, 1.5, 2.0$ : (a) using the LD method and (b) using the ACM.

Thus, by time  $t = 2.0$ , the system must return to its initial state. In this test, we test only the LD and ACM schemes that performed best in the previous problems. The calculations are performed on a  $200 \times 200$  grid. The numerical results are shown, respectively, in Figs. 17a and 17b. The interface resolution using the LD scheme is almost perfect. The ACM results in the distortion of the material interfaces.

## CONCLUSIONS

In this paper, we describe a new method for solving the system of transport equations for volume fractions of a multicomponent heterogeneous system in a specified velocity field on fixed Eulerian grids. The method ensures the following compatibility conditions for the volume fractions: (1) the volume fraction of each component should be in the range  $[0,1]$ , and (2) any partial sum of volume fractions should not exceed unity. In this case, the method is compatible with various TVD schemes and interface-sharpening methods. The method is simple and does not require significant changes in the schemes applied. It is tested on different problems with the MUSCL (with Minmod, van Leer, van Albada, Superbee limiters), THINC, LD, AntiD, and AMC schemes. The best interface resolution properties were obtained using the LD scheme. The method can be applied to the interface-capturing calculation (on fixed Eulerian grids) of incompressible and compressible flows of multiphase media with interfaces, which will be the subject of our future work.

## CONFLICT OF INTEREST

The authors declare that they have no conflict of interest.

## REFERENCES

1. S. Galera, P. H. Maire, and J. Breil, “A two-dimensional unstructured cell-centered multi-material ALE scheme using VOF interface reconstruction,” *J. Comput. Phys.* **229**, 5755–5787 (2010).
2. P. H. Maire, R. Abgrall, J. Breil, and J. Ovadia, “A cell-centered lagrangian scheme for two-dimensional compressible flow problems,” *SIAM J. Sci. Comput.* **29**, 1781–1824 (2007).
3. J. Glimm, X. L. Li, Y. J. Liu, Z. L. Xu, and N. Zhao, “Conservative front tracking with improved accuracy,” *SIAM J. Numer. Anal.* **41**, 1926–1947 (2003).
4. H. Terashima and G. Tryggvason, “A front-tracking/ghost-fluid method for fluid interfaces in compressible flows,” *J. Comput. Phys.* **228**, 4012–4037 (2009).
5. W. Mulder, S. Osher, and J. A. Sethian, “Computing interface motion in compressible gas dynamics,” *J. Comput. Phys.* **100**, 209–228 (1992).
6. R. Abgrall, “How to prevent pressure oscillations in multicomponent flow calculations: a quasi-conservative approach,” *J. Comput. Phys.* **125**, 150–160 (1996).
7. R. Saurel and R. Abgrall, “A multiphase Godunov method for compressible multifluid and multiphase flows,” *J. Comput. Phys.* **150** (2), 425–467 (1999).
8. I. Menshov and P. Zakharov, “On the composite Riemann problem for multi-material fluid flows,” *Int. J. Numer. Methods Fluids* **76**, 109–127 (2014).
9. G. Allaire, S. Clerc, and S. Kokh, “A five-equation model for the simulation of interfaces between compressible fluids,” *J. Comput. Phys.* **181**, 577–616 (2002).
10. S. Jaouen and F. Lagoutière, “Numerical transport of an arbitrary number of components,” *Comput. Methods Appl. Math.* **196**, 3127–3140 (2007).
11. B. Després and F. Lagoutière, “Contact discontinuity capturing schemes for linear advection, compressible gas dynamics,” *J. Sci. Comput.* **16**, 479–524 (2001).
12. F. Xiao, Y. Honma, and T. Kono, “A simple algebraic interface capturing scheme using hyperbolic tangent function,” *Int. J. Numer. Mech. Fluids* **48**, 1023–1040 (2005).
13. K. K. So, X. Y. Hu, and N. A. Adams, “Anti-diffusion method for interface steepening in two-phase incompressible flow,” *J. Comput. Phys.* **230**, 5155–5177 (2011).
14. K. K. So, X. Y. Hu, and N. A. Adams, “Anti-diffusion interface sharpening technique for two-phase compressible flow simulations,” *J. Comput. Phys.* **231**, 4304–4323 (2012).
15. A. Harten, “The artificial compression method for computation of shocks and contact discontinuities, I: Single conservation laws,” *Commun. Pure Appl. Math* **30**, 611–638 (1977).
16. A. Harten, “The artificial compression method for computation of shocks and contact discontinuities, III: Self-adjusting hybrid schemes,” *Math. Comput.* **32**, 363–389 (1978).

*Translated by A. Ivanov*